Solar and thermal radiation profiles and radiative forcing measured through the atmosphere

Rolf Philipona,[1] Andreas Kräuchi,[2] and Emmanuel Brocard[1]

Received 19 April 2012; revised 11 June 2012; accepted 11 June 2012; published 11 July 2012.

[1] Solar shortwave and thermal longwave radiation at the Earth's surface and at the top of the atmosphere is commonly measured at surface stations, from airplanes and from satellites. Here we show radiative flux profiles measured with radiosondes ascending from the Earth's surface to 35 km into the stratosphere. During two-hour flights solar shortwave and thermal longwave radiation are measured both downward and upward with four individual sensors. Daytime solar and thermal radiation is compared to nighttime measurements and 24-hour average radiation budget profiles are shown through the atmosphere. However, of even greater importance with regard to climate change are measured upward and downward longwave greenhouse radiation profiles. Their changes with temperature and water vapor enable direct measurement of radiative forcing through the atmosphere. Measurements during two cloud-free nights with different temperature and different water vapor amount, show an almost equal but opposite net longwave radiation change, or water vapor greenhouse forcing, downwards to the surface and upward into space. Radiative flux profiles clearly illustrate the Earth's atmospheric greenhouse effect, and allow important investigations of clouds and other atmospheric constituents and their effects on shortwave reflection, as well as longwave emission towards the surface and into space.
Citation: Philipona, R., A. Kräuchi, and E. Brocard (2012), Solar and thermal radiation profiles and radiative forcing measured through the atmosphere, *Geophys. Res. Lett.*, *39*, L13806, doi:10.1029/2012GL052087.

1. Introduction

[2] Solar shortwave radiation at the Earth's surface has been quantitatively measured for more than a century [*Fröhlich*, 1991]. Thermal longwave radiation is reliably measured at the surface since the 1990s [*Ohmura et al.*, 1998; *Philipona et al.*, 2001], and increasing longwave fluxes with rising temperatures have been observed [*Philipona et al.*, 2004; *Wild et al.*, 2008]. Total solar irradiance (*TSI*) is measured from space since 1979 [*Willson*, 1997; *Fröhlich and Lean*, 2004], and composite time-series are available over three solar cycles [*Foukal et al.*, 2006; *Kopp and Lean*, 2011]. Radiance spectra at the top of the atmosphere and at the Earth's surface are measured from satellites since the late 1960s, allowing for estimations of the radiation budget and for investigations of radiative climate forcing in the Earth-atmosphere system [*Raschke et al.*, 1973; *Ramanathan et al.*, 1989; *Trenberth et al.*, 2009]. Irradiance and actinic flux measurements have been made from airplanes, primarily for shortwave absorption studies [*Valero et al.*, 1997; *Junkermann et al.*, 2002]. Vertical radiation profiles through the atmosphere on the other hand, were sporadically measured with rather simple instruments around the 1950s [*Suomi et al.*, 1958], and later in only few experiments at divers locations in the world [*Paltridge and Sargent*, 1971; *Yamamoto et al.*, 1995; *Asano et al.*, 2004].

[3] However, upper-air observations for climate have recently been given more attention with the initiation of the GCOS (Global Climate Observing System) Reference Upper Air Network (GRUAN) to provide climate-quality measurements of tropospheric and lower stratospheric variables [*Global Climate Observing System* (*GCOS*), 2007; *Seidel et al.*, 2009]. GRUAN's goal is to feature measurements of the "Essential Climate Variables" identified by *GCOS* [2010] with a focus on upper-air variables. The primary objectives are to monitor changes in temperature profiles and to characterize water vapor in the upper troposphere and lower stratosphere (UTLS) [*Thorne et al.*, 2005; *Randel et al.*, 2006]. Both temperature and water vapor changes in the atmosphere alter radiative fluxes, and in relation with surface trends, are crucial for the understanding of climate change [*Hansen et al.*, 2005]. The enhanced greenhouse effect of a given increase in water vapor in the UTLS appears to be larger than in the lower troposphere [*Held and Soden*, 2000]. Also, clouds and particularly high clouds caused by water vapor in this region affect both the planet's shortwave albedo and longwave radiative transfer as well as emission to space and hence the greenhouse effect [*Ohring and Clapp*, 1980; *Eyring et al.*, 2005] . However, these topics need further investigations, and direct in-situ measurements of radiative fluxes through the atmosphere and particularly the UTLS produce valuable information and provide a more direct way to measure and understand radiative forcing and the greenhouse effect.

[4] Here we show solar and greenhouse radiation profiles measured in cloud-free conditions, in-situ through the troposphere and into the stratosphere. Solar shortwave and thermal longwave radiation profiles - downward and upward - from a day and a night flight on 23 September 2011 are shown, and 24-hour average radiation budget profiles are presented. An additional night flight on 9 September allows specific longwave radiation comparisons with the flight on 23 September. The two nights, which showed different temperature and humidity throughout the troposphere, allow quantifying the longwave radiative forcing at the surface and

[1]MeteoSwiss, Federal Office of Meteorology and Climatology, Payerne, Switzerland.
[2]Institute for Atmospheric and Climate Science, ETH Zurich, Zurich, Switzerland.

Corresponding author: R. Philipona, MeteoSwiss, Federal Office of Meteorology and Climatology, Aerological Station, CH-1530 Payerne, Switzerland. (rolf.philipona@meteoswiss.ch)

0094-8276/12/2012GL052087

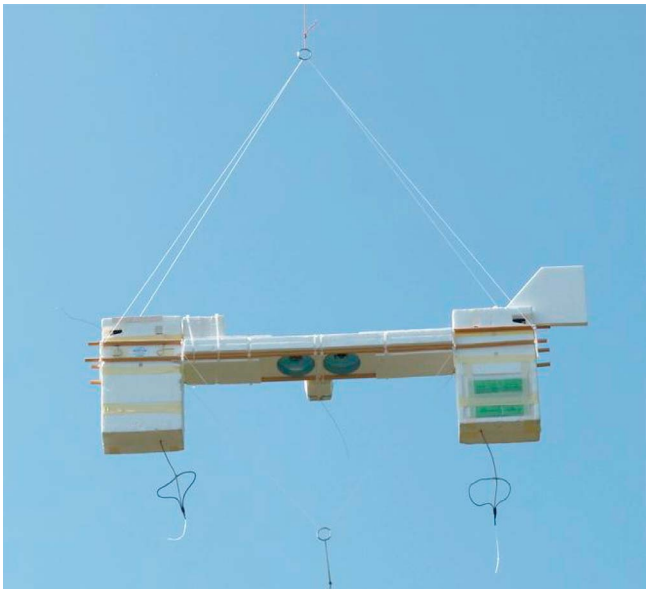

Figure 1. Radiometer radiosonde package. The package consists of two SRS-C34 radiosondes at each end and of the CNR4 with up- and down-facing pyranometers and pyrgeometers in the center. A Vaisala RS92 radiosonde is fixed behind the CNR4 for temperature and humidity comparisons. The SRS-C34 on the left records all thermopile voltages and instrument temperatures of the CNR4, and the one on the right is used for radiation effect experiments. A video camera is mounted upward beside the left SRS-C34.

the top of the atmosphere, and clearly illustrate and demonstrate cause and effect of the atmospheric greenhouse warming.

2. Upper-Air Solar and Thermal Radiometry

[5] We use a Global Positioning System (GPS) equipped digital Meteolabor SRS-C34 radiosonde, which measures air temperature and humidity, and features additional channels measuring four thermopile voltages and several instrument temperatures of the modified Kipp & Zonen CNR4 net radiometer. The CNR4 consists of two pyranometers for measuring downward and upward solar shortwave radiation, and two pyrgeometers for measuring upward and downward thermal longwave radiation. All body and dome temperatures of the radiometers are measured with the same type of thermocouple as used for air temperature measurement on the SRS-C34. Precise body and dome temperature measurements are crucial and allow for corrections of differential thermal emissions between the radiometer domes and the thermopile, which result from large temperature gradients, when the instrument cools from +20°C at the surface down to −60°C in the stratosphere.

[6] The CNR4 is mounted between two SRS-C34 radiosondes (Figure 1). The sonde package also carries a Vaisala RS92 radiosonde for temperature and humidity comparisons and a video camera to monitor the flight. A new technique is used to lift the radiosonde package, consisting of two balloons and an aluminum triangle equipped with a GPS controlled mechanism which allows automatic release of the larger carrier balloon at a pre-set altitude. The two balloons are inflated such as to lift the payload at a constant climbing rate of about 5 m/s from the aerological station in Payerne, Switzerland to above 30 km (Payerne coordinates: E 6.9440°; N 46.8130°; Alt 491 m asl., summer time is GMT+2). During the two-hour ascent, the radiosonde makes a horizontal displacement of 30 to 50 km and transmits the measured signals at 1 s resolution to the ground. After the release of the carrier balloon, the sonde descends with the smaller parachute balloon.

[7] First test flights were made during summer 2011, under cloud-free and synoptically quiet conditions, which allowed reliable flight trajectory forecasts and successful recovery of the radiosonde. Measurements under cloud-free conditions are basic for the understanding and illustration of the greenhouse radiation and can be compared to model calculations. The four radiometers are pre-calibrated and compared to surface radiation measurements at the on-site Payerne Baseline Surface Radiation Network (BSRN) station before launch. Measurement uncertainty is traced to BSRN standards, which is in the order of 1%, hence, ± 4 W m^{-2} for longwave and ± 10 W m^{-2} for shortwave radiation. All measurements presented were made with the same instrument; hence differences shown between flights have uncertainties of ± 2 W m^{-2}. While the upward facing instruments have a hemispheric field of view angle of 180 degrees, the downward facing instruments are limited to a field of view angle of 120 degrees. However, all measurements are made with the same limited field of view angle and the instruments are calibrated against hemispheric viewing instruments at the BSRN site. The CNR4 is adjusted horizontally before start, and the double balloon technique has the important advantage to guarantee very quiet ascents without pendulum motions, which are usually observed on single balloon flights. Hence, the pyranometers and pyrgeometers measure hemispheric solar and thermal irradiance from above and from below in W m^{-2}. By convention all downward fluxes are positive and upward fluxes are negative. Net radiation is the sum of downward and upward fluxes.

3. Surface Radiation and Upper-Air Profiles

[8] Shortwave downward radiation (*SDR*) and shortwave upward radiation (*SUR*) as well as longwave downward radiation (*LDR*) and longwave upward radiation (*LUR*) measured at the BSRN tower 10 m above ground are shown in one minute resolution over 24 hours on 23 September (Figure 2a). Shortwave net radiation (*SNR*) and longwave net radiation (*LNR*) fluxes are also shown. The shortwave fluxes indicate some scattered clouds in the morning and early afternoon. The daytime upper-air radiometry sounding was launched at UT 10:13. The sonde was recovered in the afternoon and launched again from Payerne at night at UT 21:20.

[9] Upper-air radiation profiles for the day and the night flight are shown in Figure 2b. The daytime shortwave downward radiation (*SDR_d*) shows about +680 W m^{-2} at the surface and +880 W m^{-2} at 32 km. This altitude was reached at UT 12:30. The solar height at the sonde's location was 40.92 degrees, resulting in a direct solar component of +1344 W m^{-2}. This is more than 99% of the direct solar irradiance of 1352 W m^{-2} above the atmosphere on

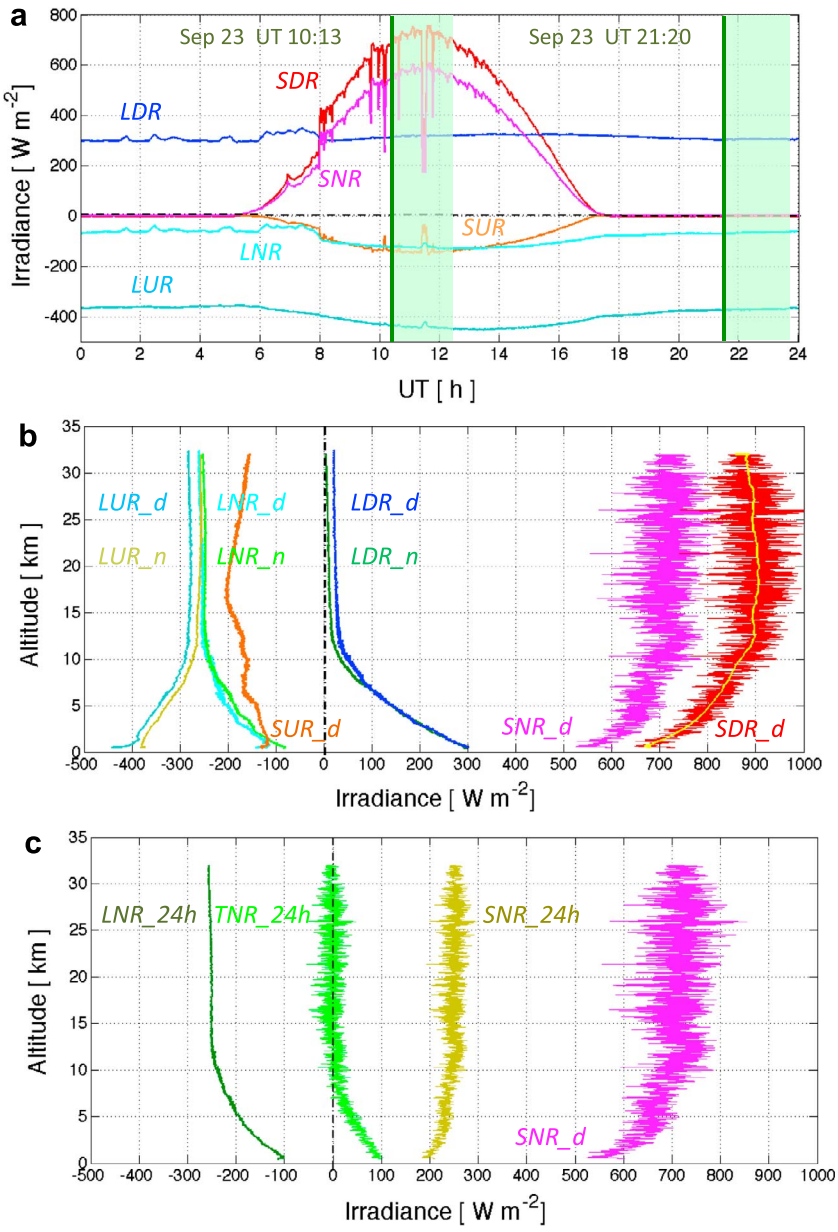

Figure 2. Surface and upper-air radiative flux measurements in Payerne. (a) Surface shortwave (*SDR*) and longwave (*LDR*) downward radiation, shortwave (*SUR*) and longwave (*LUR*) upward radiation and shortwave (*SNR*) and longwave (*LNR*) net radiation fluxes measured 10 m above ground at the Payerne BSRN station during the 24 hours of 23 September 2011. Upper-air radiometry sondes were launched at UT 10:13 (daytime) and at UT 21:20 (nighttime), each taking about 2 hours to reach 32 km. (b) Radiation flux profiles measured during daytime (*NAME_d*) and nighttime (*NAME_n*) soundings. To fit a smoothing curve to *SDR_d* a locally weighted least squares regression technique is used (yellow line). (c) 24-hour averaged shortwave (*SNR_24h*), longwave (*LNR_24h*) and total (*TNR_24h*) net radiation flux profiles.

23 September (*TSI* = 1362 W m^{-2}). The measured *SDR_d* signal is rather noisy due to the rotation of the sonde, and to fit a smoothing curve to the dataset a locally weighted least squares regression technique is used (yellow line). *SDR_d* strongly increases up to the tropopause (∼12 km altitude), but shows small changes above. The shortwave upward radiation (*SUR_d*) shows about −130 W m^{-2} at the surface and −160 W m^{-2} at 32 km. It shows variations with altitude due to changing scattered clouds below. The shortwave net radiation (*SNR_d*) results in +550 W m^{-2} at the surface and +720 W m^{-2} at 32 km. The shortwave measurements reveal that around solar noon 18% of solar radiation was reflected back to space by the atmosphere and the surface, 19% was absorbed in the atmosphere and 63% was absorbed at the ground.

[10] The surface-emitted longwave upward radiation is about −445 W m^{-2} during the day (*LUR_d*) but only −380 W m^{-2} during the night (*LUR_n*). However, *LUR_d* shows a strong decrease during the first 1,000 m and then decreases to about −280 W m^{-2} at the tropopause. *LUR_n*

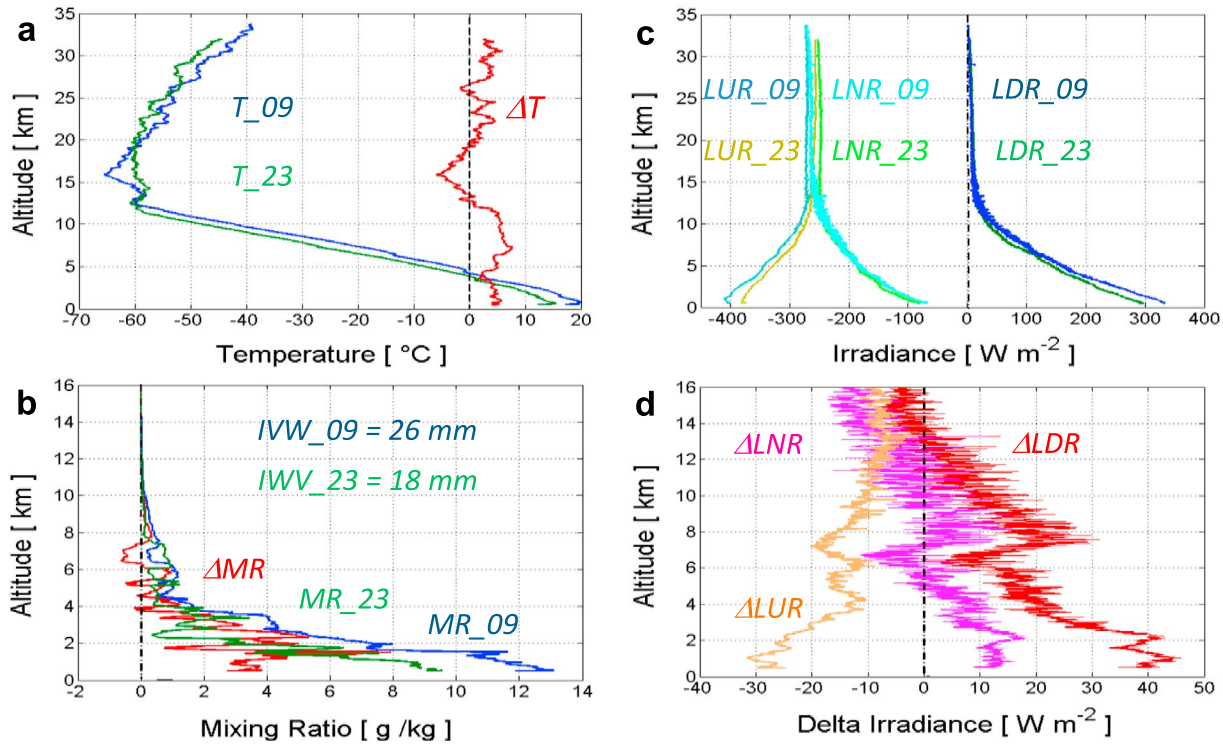

Figure 3. Temperature, humidity mixing ratio and longwave radiation profiles measured during the nights of 9 and 23 September 2011. (a) Temperature on 9 September (*T*_09) and on 23 September (*T*_23) and difference ΔT. (b) Humidity mixing ratio (*MR*_09) and (*MR*_23) and difference (ΔMR). (c) Longwave radiation: downward (*LDR*_09) and (*LDR*_23), upward (*LUR*_09) and (*LUR*_23), and net (*LNR*_09) and (*LNR*_23). (d) Longwave radiation differences between 9 and 23 September: downward (ΔLDR), upward (ΔLUR) and net (ΔLNR).

decreases similarly and above the tropopause *LUR_d* and *LUR_n* stay fairly constant with the night emission about 20 W m^{-2} lower. *LDR_d* is similar to *LDR_n* in the lower troposphere, decreasing from about +300 W m^{-2} at the surface down to about +15 W m^{-2} at the tropopause. Above the tropopause, *LDR_n* decreases steadily down to +4 W m^{-2} at 32 km. However, *LDR_d* is always about 15 W m^{-2} higher even at 32 km. This difference, which is observable from above 7 km is due to thermal longwave radiation from the Sun. *LNR_d* at the surface is about −140 W m^{-2}, whereas during the night *LNR_n* is only about −80 W m^{-2}. However, the difference decreases with height and at 32 km day and night net emissions are −270 W m^{-2} and −260 W m^{-2}, respectively.

[11] In Figure 2c we show the radiation budget through the atmosphere averaged over the 24 hours of 23 September. The shortwave net radiation profile over 24 hours (*SNR_24h*) represents the average *SNR* flux, which corresponds to the integrated solar energy received over the 24 hours. Longwave net radiation daily average (*LNR_24h*) is the average between *LNR_d* and *LNR_n*. The sum of the *SNR_24h* and *LNR_24h* profiles finally results in the total net radiation daily average profile (*TNR_24h*), which illustrates the radiation budget at the surface and in the atmosphere. At the surface *TNR_24h* shows about +100 W m^{-2}. This net radiative energy is available to heat the ground, to heat the surface air and to evaporate water. The largest part rises as latent and sensible heat fluxes into the troposphere and only a small part is absorbed for the ground fluxes. *TNR_24h* decreases with altitude according to the decrease of the latent and sensible heat fluxes and hence water vapor in the atmosphere.

4. Greenhouse Effect and Radiative Forcing

[12] In Figure 3 we compare the two night flights of 9 September (up to 34 km) and of 23 September (up to 32 km) and show the relation between temperature, humidity and longwave radiation. Both nights were cloud-free, but the surface temperature measured at the meteorological station Payerne on 9 Sep was 5°C higher, and a similar difference was measured throughout the troposphere (Figure 3a). Atmospheric humidity, shown as mixing ratio only up to 16 km (Figure 3b), was also higher on 9 Sep except in a layer between 6 and 7 km. The integrated water vapor (*IWV*), which is measured by an on-site GPS receiver, was 26 mm on 9 Sep and only 18 mm on 23 Sep. Hence, *IWV* decreased by 7.3% K^{-1} from 9 Sep to 23 Sep, which is in good agreement with the Clausius-Clapeyron relation [*O'Gorman and Muller*, 2010].

[13] The longwave upward radiation emitted at the surface was in the order of −400 W m^{-2} in both nights and the emission into space was around −280 W m^{-2} (Figure 3c). The difference ΔLUR between 9 Sep and 23 Sep was −28 W m^{-2} at the surface (Figure 3d), which is in good agreement with the difference between thermal emissions ($\varepsilon\sigma T^4$) at surface temperatures of +16°C (9 Sep) and +11°C (23 Sep). In the troposphere, ΔLUR decreases with variations primarily due to water vapor differences in certain layers between the two

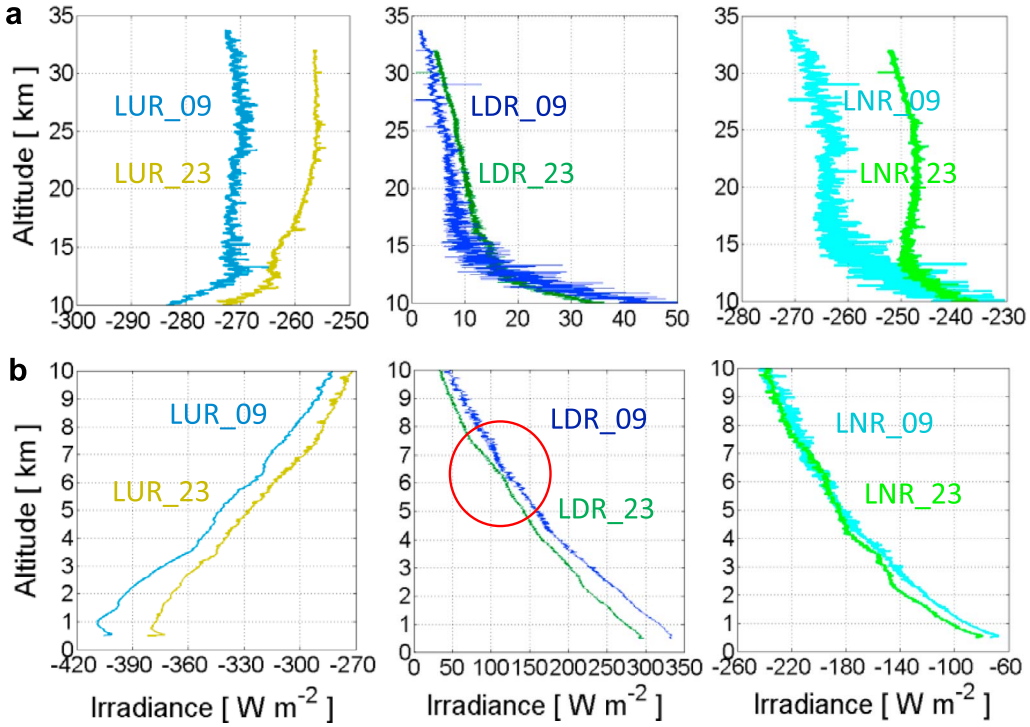

Figure 4. Details of longwave radiation profiles measured during the nights of 9 and 23 September 2011 (a) above 10 km and (b) below 10 km. Longwave radiation: downward (*LDR*_09) and (*LDR*_23), and upward (*LUR*_09) and (*LUR*_23) and net (*LNR*_09) and (*LNR*_23).

days, and reaches a minimum of about 8 W m^{-2} around the tropopause (12–13 km altitude). *LUR*_09 and *LUR*_23 (shown in more details above 10 km (Figure 4a) and below 10 km (Figure 4b)) clearly decrease up to the tropopause and are then fairly constant on 9 Sep, while still declining above 15 km on 23 Sep due to decreasing temperature at the ground surface. The greenhouse effect (*G*) has been defined as *LUR* emitted by the Earth surface minus *LUR* emitted at the top of the atmosphere [*Raval and Ramanathan*, 1989]. Using this definition *G* is +135 W m^{-2} on 9 Sep and +123 W m^{-2} on 23 Sep. However, as surface emission shows large diurnal changes these night values are not definite.

[14] The longwave downward radiation *LDR*_09 went from +332 W m^{-2} at the surface to +1.5 W m^{-2} at 34 km (Figures 3c and 4). The difference ΔLDR between 9 Sep and 23 Sep is +40 W m^{-2} at the surface (Figure 3d). Of this difference about +22 W m^{-2} is due to the higher temperature and related *LUR*_09 emission at the surface, and the rest is due to the higher water vapor in the troposphere on 9 Sep. ΔLDR then decreases to about +5 W m^{-2} at an altitude of 6–7 km, where water vapor was lower on 9 Sep and higher on 23 Sep (Figure 3b). The change of *LDR* around the water vapor layer shows that any increase or decrease in greenhouse gases produces an increase or decrease in *LDR* (Figure 4b, red circle). ΔLDR increases again above the water vapor layer and then decreases higher up and becomes zero at the tropopause. Above the tropopause *LDR*_09 decreases more than *LDR*_23 (Figure 4a), likely due to the still decreasing temperature above the tropopause on 9 Sep. Above 16 km, *LDR* decreases similarly in both nights as the sondes go through the stratospheric ozone layer and other remaining greenhouse gases. Indeed, ozone profiles from soundings in Payerne as well as water vapor profiles measured with the MIAWARA [*Deuber et al.*, 2004] instrument above 20 km altitude in Bern (30 km from Payerne, and on the flight trajectory) look very similar for both nights.

[15] The longwave net radiation in both nights is around −80 W m^{-2} at the surface and increases to around −260 W m^{-2} at 32 km (Figures 3c and 4). However, at the surface *LNR*_09 is smaller than *LNR*_23 yielding a ΔLNR of +12 W m^{-2} (Figure 3d). This shows that due to the higher temperature and water vapor on 9 Sep the longwave downward radiation changed more than the longwave upward radiation. Above the tropopause ΔLNR is about −12 W m^{-2} (at ∼15 km altitude; higher up *LUR*_23 changed due to changing ground temperature). This shows that the longwave net radiation into space also increased due to the additional water vapor and the 5°C higher temperature on 9 Sep. Hence, the comparison between the two nights demonstrates radiative forcing due to additional water vapor and temperature in the troposphere on 9 Sep through an increase of *LNR* emission into space by about 12 W m^{-2}, and an increase of *LNR* towards the ground also by about 12 W m^{-2}. *LDR* on the other hand increased by as much as 40 W m^{-2}. The measurements also enable calculating the rate of change of the radiative forcing, which shows that under cloud-free conditions *LNR* into space and *LNR* towards the surface change by about 2.4 W m^{-2} K^{-1}, whereas *LDR* changes by 8 W m^{-2} K^{-1}.

5. Summary

[16] Consistency observed between the different flights, as well as measurements of more than 99% of direct solar irradiance at 32 km and longwave downward radiation down to

1.5 W m^{-2} at 34 km show, that solar and thermal radiation can reliably be measured through the atmosphere. Radiation profiles show large changes through the troposphere. The tropopause forms a critical barrier, above which water vapor is strongly reduced and shortwave and longwave radiation show only small changes. Day and night comparison show large gradients of daytime thermal emission in the first couple of 100 m above ground, and allow determining solar absorption and the radiation budget through the atmosphere. Comparison between nights with different atmospheric temperature and corresponding water vapor demonstrate greenhouse warming or radiative forcing due to rising greenhouse gases (in this case water vapor), which result in an increase of longwave net radiation emitted into space and also in a similar increase of longwave net radiation towards the surface.

[17] The upper-air radiation profiles shown here were all measured under cloud free conditions, which is basic for greenhouse effect studies. However, future measurements through clouds, aerosols or other atmospheric constituents will allow investigating shortwave and longwave radiative effects and forcing at different altitudes. Very important for climate change issues will be investigations of clouds and water vapor changes in the UTLS and their effects on shortwave reflection and longwave emission into space.

[18] **Acknowledgments.** The authors would like to thank the radiosonde team of the MeteoSwiss aerological station at Payerne, which made the often quite difficult sonde launches and their tracking possible. We particularly thank Gonzague Romanens, Jean-Michel Cornuz and Gilbert Levrat for technical help and for launching and operating the radiosondes. We like to acknowledge Kipp & Zonen at Delft, Netherlands, which provided us with two CNR4, and Meteolabor at Wetzikon, Switzerland, for modifying the SRS-C34, which allowed flying the CNR4.

[19] The Editor thanks two anonymous reviewers for their assistance in evaluating this paper.

References

Asano, S., Y. Yoshida, Y. Miyake, and K. Nakamura (2004), Development of a radiometer-sonde for simultaneously measuring the downward and upward broadband fluxes of shortwave and longwave radiation, *J. Meteorol. Soc. Jpn.*, *82*, 623–637, doi:10.2151/jmsj.2004.623.

Deuber, B., N. Kämpfer, and D. G. Feist (2004), A new 22-GHz radiometer for middle atmospheric water vapour profile measurements, *IEEE Trans. Geosci. Remote Sens.*, *42*, 974–984.

Eyring, V., et al. (2005), A strategy for process-oriented validation of coupled chemistry climate models, *Bull. Am. Meteorol. Soc.*, *86*, 1117–1133, doi:10.1175/BAMS-86-8-1117.

Foukal, P., C. Fröhlich, H. Spruit, and T. M. L. Wigley (2006), Variations in solar luminosity and their effect on the Earth's climate, *Nature*, *443*, 161–166, doi:10.1038/nature05072.

Fröhlich, C. (1991), History of solar radiometry and the World Radiometric Reference, *Metrologia*, *28*, 111–115, doi:10.1088/0026-1394/28/3/001.

Fröhlich, C., and J. L. Lean (2004), Solar radiative output and its variability: Evidence and mechanisms, *Astron. Astrophys. Rev.*, *12*, 273–320, doi:10.1007/s00159-004-0024-1.

Global Climate Observing System (GCOS) (2007), GCOS Reference Upper-Air Network (GRUAN): Justification, requirements, siting and instrumentation options, *Rep. GCOS-112*, 25 pp., World Meteorol. Organ., Geneva, Switzerland.

Global Climate Observing System (GCOS) (2010), Implementation plan for the global observing system for climate in support of the UNFCCC (2010 update), *Rep. GCOS-138*, 179 pp., World Meteorol. Organ., Geneva, Switzerland.

Hansen, J., et al. (2005), Earth's energy imbalance: Confirmation and implications, *Science*, *308*, 1431–1435, doi:10.1126/science.1110252.

Held, I. M., and B. J. Soden (2000), Water vapor feedback and global warming, *Annu. Rev. Energy Environ.*, *25*, 441–475, doi:10.1146/annurev.energy.25.1.441.

Junkermann, W., et al. (2002), Actinic radiation and photolysis processes in the lower troposphere: Effect of clouds and aerosols, *J. Atmos. Chem.*, *42*, 413–441, doi:10.1023/A:1015774415983.

Kopp, G., and J. L. Lean (2011), A new, lower value of total solar irradiance: Evidence and climate significance, *Geophys. Res. Lett.*, *38*, L01706, doi:10.1029/2010GL045777.

O'Gorman, P. A., and C. J. Muller (2010), How closely do changes in surface and column water vapor follow Clausius-Clapeyron scaling in climate change simulations?, *Environ. Res. Lett.*, *5*, 025207, doi:10.1088/1748-9326/5/2/025207.

Ohmura, A., et al. (1998), Baseline Surface Radiation Network (BSRN/WCRP): New precision radiometry for climate research, *Bull. Am. Meteorol. Soc.*, *79*, 2115–2136, doi:10.1175/1520-0477(1998)079<2115:BSRNBW>2.0.CO;2.

Ohring, G., and P. Clapp (1980), The effect of changes in cloud amount on the net radiation at the top of the atmosphere, *J. Atmos. Sci.*, *37*, 447–454, doi:10.1175/1520-0469(1980)037<0447:TEOCIC>2.0.CO;2.

Paltridge, G. W., and S. L. Sargent (1971), Solar and thermal measurements to 32 km at low solar elevations, *J. Atmos. Sci.*, *28*, 242–253, doi:10.1175/1520-0469(1971)028<0242:SATRMT>2.0.CO;2.

Philipona, R., et al. (2001), Atmospheric longwave irradiance uncertainty: Pyrgeometers compared to an absolute sky-scanning radiometer, atmospheric emitted radiance interferometer, and radiative transfer model calculations, *J. Geophys. Res.*, *106*, 28,129–28,141, doi:10.1029/2000JD000196.

Philipona, R., B. Dürr, C. Marty, A. Ohmura, and M. Wild (2004), Radiative forcing—measured at Earth's surface—corroborate the increasing greenhouse effect, *Geophys. Res. Lett.*, *31*, L03202, doi:10.1029/2003GL018765.

Ramanathan, V., et al. (1989), Cloud radiative forcing and climate: Results from the Earth Radiation Budget Experiment, *Science*, *243*, 57–63, doi:10.1126/science.243.4887.57.

Randel, W. J., F. Wu, H. Vömel, G. E. Nedoluha, and P. Forster (2006), Decreases in stratospheric water vapor after 2001: Links to changes in the tropical tropopause and the Brewer-Dobson circulation, *J. Geophys. Res.*, *111*, D12312, doi:10.1029/2005JD006744.

Raschke, E., T. H. Vonder Haar, W. R. Bandeen, and M. Pasternak (1973), The annual radiation balance of the Earth-atmosphere system during 1969–1970 from Nimbus 3 measurements, *J. Atmos. Sci.*, *30*, 341–364, doi:10.1175/1520-0469(1973)030<0341:TARBOT>2.0.CO;2.

Raval, A., and V. Ramanathan (1989), Observational determination of the greenhouse effect, *Nature*, *342*, 758–761, doi:10.1038/342758a0.

Seidel, D. J., et al. (2009), Reference upper-air observations for climate: Rationale, progress, and plans, *Bull. Am. Meteorol. Soc.*, *90*, 361–369, doi:10.1175/2008BAMS2540.1.

Suomi, V. E., D. O. Staley, and P. M. Kuhn (1958), A direct measurement of infrared radiation divergence to 160 millibars, *Q. J. R. Meteorol. Soc.*, *84*, 134–141, doi:10.1002/qj.49708436006.

Thorne, P. W., D. E. Parker, J. R. Christy, and C. A. Mears (2005), Uncertainties in climate trends - Lessons from upper-air temperature records, *Bull. Am. Meteorol. Soc.*, *86*, 1437–1442, doi:10.1175/BAMS-86-10-1437.

Trenberth, K. E., J. T. Fasullo, and J. Kiehl (2009), Earth's global energy budget, *Bull. Am. Meteorol. Soc.*, *90*, 311–323, doi:10.1175/2008BAMS2634.1.

Valero, F. P. J., A. Bucholtz, B. C. Bush, S. K. Pope, W. D. Collins, P. Flatau, A. Strawa, and W. J. Y. Gore (1997), Atmospheric Radiation Measurements Enhanced Shortwave Experiment (ARESE): Experiment and data details, *J. Geophys. Res.*, *102*, 29,929–29,937, doi:10.1029/97JD02434.

Wild, M., J. Grieser, and C. Schär (2008), Combined surface solar brightening and increasing greenhouse effect support recent intensification of the global land-based hydrological cycle, *Geophys. Res. Lett.*, *35*, L17706, doi:10.1029/2008GL034842.

Willson, R. C. (1997), Total solar irradiance trend during solar cycles 21 and 22, *Science*, *277*, 1963–1965, doi:10.1126/science.277.5334.1963.

Yamamoto, A., T. Yamanouchi, and M. Wada (1995), Effective emissivity of clouds from radiometer measurements at Syowa station, Antarctica, *Proc. NIPR Symp. Polar Meteorol. Glaciol.*, *9*, 133–145.